Available online at www.sciencedirect.com

ScienceDirect

Mendeleev Commun., 2021, **31**, 62–64

Mendeleev Communications

Effect of the structural disorder of T-shaped triazolyl-based coordination network compounds on the pore size and stability

Min Chen,*[a,b,c] Lian-Sheng Duan[a,b,c] and Yuan-Zhen Liu*[a]

[a] *Hubei Key Laboratory of Purification and Application of Plant Anti-Cancer Active Ingredients, Hubei University of Education, 430205 Wuhan, Hubei, China. Fax: +86 278 794 3929; e-mail: chem_chenmin@163.com; liuyuanzhen@hue.edu.cn*

[b] *Hubei Engineering Technology Center of Environmental Purification Materials, University of Education, 430205 Wuhan, Hubei, China*

[c] *Research Center for Environmental Functional Materials and Pollution Control Technology, Hubei University of Education, 430205 Wuhan, Hubei, China*

DOI: 10.1016/j.mencom.2021.01.018

The coordination network compounds (CNCs) $\{[M(L_{triaz})](DMF)\}_n$ (M is Zn or Co, H_2L_{triaz} is 5-(4*H*-1,2,4-triazol-4-yl)benzene-1,3-dicarboxylic acid, and DMF is *N*,*N*-dimethylformamide) with crystallographically identifiable disorder were solvothermally synthesized. The effects of structural disorder on the pore size and stability of T-shaped triazolyl-based CNCs were determined for the first time. In contrast to isostructurally ordered ones, the pore sizes of Zn-CNC and Co-CNC changed, and the stability of Zn-CNC was improved.

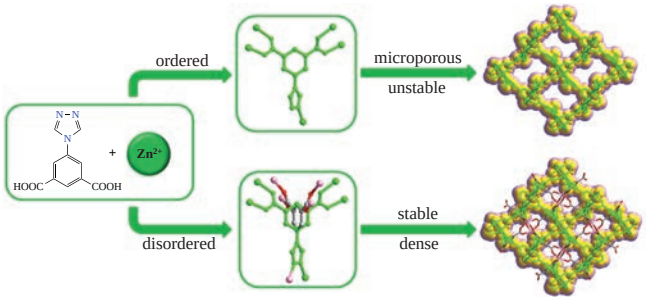

Keywords: coordination network compounds, structural disorder, pore size, stability, N_2 sorption.

Defects in coordination network compounds (CNCs), which can affect their physical and chemical properties, are of importance for tailoring material characteristics.[1–3] They include dislocations, vacancies, heterogeneities, and disorders.[1] An interesting example of disorder is NOTT-202,[4] which shows partial double interpenetration. The network fragmentation and defects allow the desolvated phase (NOTT-202a) to achieve a high specific surface area and show selective hysteretic sorption of CO_2. As the fundamental building bricks of CNCs, organic ligands are different in their charges, shapes, lengths, and functionalities.[5] Bifunctional ligands with N-containing heterocycles (such as pyridine, pyrazole, imidazole, 1,2,3-triazole, 1,2,4-triazole, and tetrazole) and carboxylate groups were popular. For example, 5-(4*H*-1,2,4-triazol-4-yl)benzene-1,3-dicarboxylic acid (H_2L_{triaz}) has been widely applied to construct CNCs with monometallic[6–20] or bimetallic ions.[21,22] Prelviously, we investigated the coordination of Zn^{2+} and Co^{2+} ions with H_2L_{triaz} in water under different reaction conditions (temperature, induction agent, and pH).[19,20] In this work, we synthesized two three-dimensional (3D) CNCs with structural disorder based on H_2L_{triaz}, Zn-CNC and Co-CNC under solvothermal conditions† and studied the effects of structural disorder on the pore size and stability.

The single crystal structure analysis‡ revealed that both Zn-CNC and Co-CNC crystallize in the monoclinic space group $P2_1/c$ and show disordered characteristics. We failed to obtain the same topologically ordered frameworks by adjusting reaction conditions including solvent, temperature, or metal source, whereas the isostructurally ordered frameworks of L_{triaz}–Mn,[6] DIRDIF-99.[25] The metal atoms and phenyl and carboxylate groups were observed in both CNCs to lie disordered across two positions with different site occupancies [0.783(7) and 0.217(7) for Zn-CNC; 0.721(2) and 0.279(2) for Co-CNC]. All hydrogen atoms were generated geometrically and refined isotropically as riding. The selected bond lengths and angles are listed in Table S1 in Online Supplementary Materials. $\{[Zn(L_{triaz})](DMF)\}_n$, M = 369.65, monoclinic, $P2_1/c$, a = 10.939(4), b = 12.157(5) and c = 14.450(6) Å, β = 110.232(14)°, V = 1803.0(13) Å^3, Z = 4, d_{calc} = 1.414 g cm^{-3}, μ = 1.394 mm^{-1}, R_{int} = 0.1630, $F(000)$ = 783, GOF = 1.694, R_1 = 0.1911, wR_2 = 0.4571 [$I > 2\sigma(I)$]. $\{[Co(L_{triaz})](DMF)\}_n$, M = 363.20, monoclinic, $P2_1/c$, a = 10.977(5), b = 11.819(4) and c = 14.682(5) Å, β = 109.648(14)°, V = 1793.9(12) Å^3, Z = 4, d_{calc} = 1.345 g cm^{-3}, μ = 0.983 mm^{-1}, R_{int} = 0.1537, $F(000)$ = 740, GOF = 1.200, R_1 = 0.1227, wR_2 = 0.3293 [$I > 2\sigma(I)$].

CCDC 2026567 and 2025459 contain the supplementary crystallographic data for this paper. The data can be obtained free of charge from The Cambridge Crystallographic Data Centre *via* http://www.ccdc.cam.ac.uk.

† Commercial reagents and solvents were used as received. The ligand H_2L_{triaz} was synthesized according to a published procedure.[23] A mixture of $MCl_2 \cdot xH_2O$ (0.1 mmol; x = 0 for Zn–CNC; x = 6 for Co-CNC), H_2L_{triaz} (0.1 mmol), and DMF (6 ml) was placed in a Teflon-lined stainless steel vessel (23 ml), heated to 120 °C for three days and then cooled to room temperature. Single crystals of Zn-CNC and Co-CNC suitable for X-ray diffraction analysis were obtained. For Zn-CNC, yield: 43%. Found (%): C, 42.42; H, 3.08; N, 14.97. Calc. for $C_{13}H_{12}N_4O_5Zn$ (%): C, 42.24; H, 3.27; N, 15.16. IR (KBr pellet, cm^{-1}): 3406 (m, br), 1624 (m), 1581 (s), 1364 (s), 1103 (m), 776 (m), 737 (m), 650 (w), 483 (w). For Co-CNC, yield: 52%. Found (%): C, 42.84; H, 3.27; N, 15.31. Calc. for $C_{13}H_{12}N_4O_5Co$ (%): C, 42.99; H, 3.33; N, 15.43. IR (KBr pellet, cm^{-1}): 3405 (m, br), 1626 (s), 1583 (s), 1387 (s), 1294 (w), 1249 (w), 1168 (w), 1100 (w), 1059 (w), 783 (m), 720 (m), 660 (w), 645 (w), 480 (w).

‡ *Crystal data*. Structural data for Zn-CNC and Co-CNC were collected on a Rigaku RAXIS-RAPID II imaging plate area detector with MoKα radiation (0.71075 Å) at 200 K. The structures were solved by direct methods with SIR92[24] and expanded using Fourier techniques by

L_{triaz}–Cu,[7,12,13] and L_{triaz}–Zn[11] were reported (Figure S1 and Table S2 in Online Supplementary Materials). In the ordered structures, the paddle-wheel second-building units (SBUs) are linked by the isophthalate units of L_{triaz} to form a square-grid **sql** layer. The two-dimensional (2D) layers are further pillared by the triazolyl units of L_{triaz} to produce a 3D **rtl** network with one-dimensional (1D) channels viewed along the *a* axis (Figure S1). However, in the disordered Zn-CNC and Co-CNC, both paddle-wheel SBUs and the isophthalate unit of L_{triaz} are composed of two disordered occupied positions A and B in different crystallographic occupancies [0.783(7) and 0.217(7) for Zn-CNC; 0.721(2) and 0.279(2) for Co-CNC] (Figure 1). Each disordered isophthalate unit of position B does not change the conformation, but it rotates a certain angle in relation to position A (Figures 1 and S2). The dihedral angles between the benzene rings of positions A and B are 85.55 and 87.36° for Zn-CNC and Co-CNC (Figure S2), respectively. Each paddle-wheel SBU of position B is closely related to the neighboring triazolyl unit of position A after the rotation (Figure S3). A distance between the metal ion from position B and the nitrogen atom from position A falls in the bonding range of coordination bond (2.153 Å for Zn-CNC and 2.119 Å for Co-CNC) (Figure S3). We believe that the formation of coordination bonds between the metal ion from position B and the nitrogen atom from position A is very likely. In this sense, the final framework is considered to consist of two interwoven **rtl** networks (see Figure 1). Thus, the Zn-CNC and Co-CNC are classified as dense frameworks. The PLATON[26] analysis (1.8 Å probe radius) indicated that the effective free volumes (after removing the lattice guest solvents) are 350.4 $Å^3$ (19.4% per unit cell) in Zn-CNC and 363.1 $Å^3$ (20.2% per unit cell) in Co-CNC (Table S2). The same analysis for the ordered structures of L_{triaz}–Mn,[6] L_{triaz}–Cu,[7,12,13] and L_{triaz}–Zn[11] showed that their overall free voids ranged from 41.1 to 47.3% per unit cell, and they were almost twice as high as those of disordered structures (Table S2).

To evaluate the stability and porosity of Zn-CNC and Co-CNC, thermogravimetric analysis (TGA), power X-ray diffraction (PXRD), and physical nitrogen measurements were performed. The characteristic diffraction peaks of as-synthesized bulk Zn-CNC and Co-CNC samples were closely coincident with those of simulated patterns from the single-crystal data, which were indicative of the phase purity and air stability (Figure S4). A slight migration between the simulated and as-synthesized patterns was attributed to the thermal expansion of crystal lattices at room temperature (of the PXRD measurements) compared to 200 K (the temperature of a single-crystal X-ray study). The TGA curves of as-synthesized samples had no obvious signals to confirm the collapse temperatures of Zn-CNC and Co-CNC (Figure S5). For the removal of DMF solvent molecules prior to porosity analysis, the as-synthesized samples were soaked in CH_2Cl_2 for 48 h and fresh CH_2Cl_2 portions were changed every 12 h. The main diffraction peaks of the CH_2Cl_2-exchanged samples of Zn-CNC and Co-CNC moved toward high angles, as compared to as-synthesized ones (Figure S4); this fact can be explained by the lattice contraction because of the escape of CH_2Cl_2 trapped in the pore space. The merge of peaks indicated a slight decrease of crystallinity. Nevertheless, the PXRD patterns still can validate the structural integrities of the CH_2Cl_2-exchanged samples. The TGA curves of both CH_2Cl_2-exchanged samples showed obvious plateau regions from ~150 °C, and the final weight losses were observed at about 400 °C owing to the collapse of the frameworks (Figure S5). Then, the activated samples were obtained by heating the CH_2Cl_2-exchanged samples in a high vacuum ($<10^{-5}$ Torr) at 100 °C overnight. The TGA curves (Figure S5) confirmed the complete removal of residual solvents from the CNCs. An uneven baseline of the PXRD patterns of activated samples indicates a further decrease in the crystallinity but no notable structural changes. As depicted in Figure 2, the N_2 sorption isotherms for Zn-CNC and Co-CNC show no increase near the saturation pressure region of P/P_0 = 0.01, but a very sharp increase without hysteresis loops at P/P_0 from 0.9 to 1.0 was observed. The type II behaviors[27] mentioned above indicate the absence of porous structures from Zn-CNC and Co-CNC.

The previously reported ordered L_{triaz}–Mn[6] and L_{triaz}–Cu[7,12,13] are isostructural with Zn-CNC and Co-CNC, however their metal sources are different. The ordered L_{triaz}–Zn,[11] which was obtained by a reaction of H_2L_{triaz} with $Zn(NO_3)_2 \cdot 6H_2O$ at 80 °C in NMP–MeOH, provided a good example for comparing to Zn-CNC. The PXRD patterns of the as-synthesized sample of L_{triaz}–Zn soaked in MeOH or CH_2Cl_2 revealed a loss of the crystallinity, indicating its instability. However, the disordered Zn-CNC showed higher stability after both solvent exchange and vacuum heating (Figure S4). We believe that the high possibility of coordination bonding between the paddle-wheel SBU of position B and the adjacent triazolyl unit of position A in Zn-CNC has an essential effect on its stability. Based on the same consideration, the final structure can be imagined as two interwoven **rtl** networks, which form a dense structure, as confirmed by the N_2 sorption isotherm. According to Su and co-workers, a similar disordered isoreticular **rtl** MOF (L_{imi}–Cu) based on 5-(1*H*-imidazol-1-yl)isophthalate acid was observed. A comparison of structural disorders in Zn-CNC (or Co-CNC) and L_{imi}–Cu offers the following differences. (i) The disordered parts of ligands are different. Only the isophthalate unit of L_{triaz} is disordered in Zn-CNC (or Co-CNC), while both isophthalate and imidazolyl units of L_{imi} are disordered in L_{imi}–Cu. (ii) The possibility of formation of new coordination bonds between two disordered parts is different. The distance between each terminal nitrogen atom in the triazolyl unit of L_{triaz} and an adjacent metal atom from the disordered occupied position is sufficiently close for the formation of a normal coordination bond (Figure S3). The only terminal nitrogen atom in the imidazolyl unit of L_{imi} can coordinate with only one metal atom, so the possibility of formation of a new coordination linkage is almost zero (Figure S3). In this sense, the structural disorder leads to offset

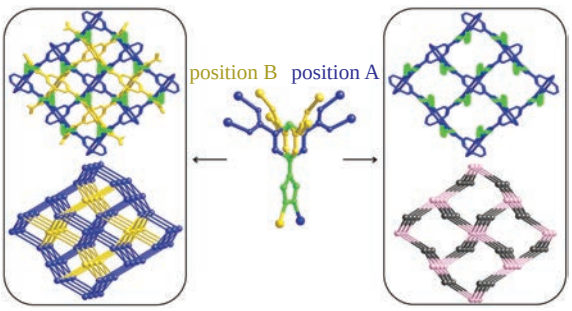

Figure 1 Disordered *versus* ordered framework for L_{triaz}–M (M = Mn, Cu, Zn, or Co).

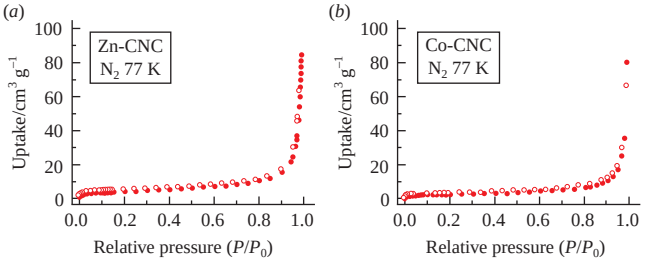

Figure 2 Nitrogen sorption isotherms at 77 K for (*a*) Zn-CNC and (*b*) Co-CNC (closed and open circles refer to adsorption and desorption, respectively).

stacking of 2D **sql** sheets in both Zn-CNC (or Co-CNC) and L_{imi}–Cu, while the effects on pore sizes are different. The interlayer slips in L_{imi}–Cu produces different pore permeability, while the possible new coordination linkages in each layer reduce the pore sizes and result in a dense framework of Zn-CNC (or Co-CNC). From the above comparison and contrast, the introduction of structural disorder disrupts the regular porous interior of CNCs, and the pore size and stability can be drastically altered compared to those of the ordered isostructural CNCs.

In summary, two **rtl**-CNCs (Zn-CNC and Co-CNC) with structural disorder were prepared based on the T-shaped ligand with an amalgamation of 1,2,4-triazole and carboxylate units and characterized. The results of this work illustrate the significance of structural disorder in the modification of the properties of materials.

This work was supported by the Natural Science Foundation of Hubei Province (2019CFB785).

Online Supplementary Materials

Supplementary data associated with this article can be found in the online version at doi: 10.1016/j.mencom.2021.01.018.

References

1 Z. Fang, B. Bueken, D. E. De Vos and R. A. Fischer, *Angew. Chem., Int. Ed.*, 2015, **54**, 7234.
2 A. K. Cheetham, T. D. Bennett, F.-X. Coudert and A. L. Goodwin, *Dalton Trans.*, 2016, **45**, 4113.
3 O. Halbherr and R. A. Fischer, in *The Chemistry of Metal-Organic Frameworks: Synthesis, Characterization, and Applications*, ed. S. Kaskel, Wiley, Weinheim, 2016, pp. 795–822.
4 S. Yang, X. Lin, W. Lewis, M. Suyetin, E. Bichoutskaia, J. E. Parker, C. C. Tang, D. R. Allan, P. J. Rizkallah, P. Hubberstey, N. R. Champness, K. M. Thomas, A. J. Blake and M. Schröder, *Nat. Mater.*, 2012, **11**, 710.
5 L. M. Kustov, V. I. Isaeva, J. Přech and K. K. Bisht, *Mendeleev Commun.*, 2019, **29**, 361.
6 T. Panda, P. Pachfule and R. Banerjee, *Chem. Commun.*, 2011, **47**, 7674.
7 J. F. Eubank, L. Wojtas, M. R. Hight, T. Bousquet, V. Ch. Kravtsov and M. Eddaoudi, *J. Am. Chem. Soc.*, 2011, **133**, 17532.
8 T. Panda, T. Kundu and R. Banerjee, *Chem. Commun.*, 2012, **48**, 5464.
9 L. Wen, W. Shi, X. Chen, H. Li and P. Cheng, *Eur. J. Inorg. Chem.*, 2012, 3562.
10 A. Mallick, E.-M. Schön, T. Panda, K. Sreenivas, D. D. Díaz and R. Banerjee, *J. Mater. Chem.*, 2012, **22**, 14951.
11 D.-M. Chen, X.-Z. Ma, W. Shi and P. Cheng, *Cryst. Growth Des.*, 2015, **15**, 3999.
12 Z. Yao, Z. Zhang, L. Liu, Z. Li, W. Zhou, Y. Zhao, Y. Han, B. Chen, R. Krishna and S. Xiang, *Chem. – Eur. J.*, 2016, **22**, 5676.
13 M. Kobalz, J. Lincke, K. Kobalz, O. Erhart, J. Bergmann, D. Lässig, M. Lange, J. Möllmer, R. Gläser, R. Staudt and H. Krautscheid, *Inorg. Chem.*, 2016, **55**, 3030.
14 L. Wang, G. Fan, X. Xu, D. Chen, L. Wang, W. Shi and P. Cheng, *J. Mater. Chem. A*, 2017, **5**, 5541.
15 W.-H. Wang, Q. Gao, A.-L. Li, Y.-Y. Jia, S.-Y. Zhang, J.-H. Wang, Y.-H. Zhang and X.-H. Bu, *Chin. Chem. Lett.*, 2018, **29**, 336.
16 J. Yuan, J. Li, L. Kan, L. Zou, J. Zhao, D.-S. Li, G. Li, L. Zhang and Y. Liu, *Cryst. Growth Des.*, 2018, **18**, 5449.
17 H. Jiang, J. Jia, A. Shkurenko, Z. Chen, K. Adil, Y. Belmabkhout, L. J. Weselinski, A. H. Assen, D.-X. Xue, M. O'Keeffe and M. Eddaoudi, *J. Am. Chem. Soc.*, 2018, **140**, 8858.
18 W. Wang, Q. Gao, X. Li, J. Wang, C. Wang, Y. Zhang and X. Bu, *Chin. Chem. Lett.*, 2019, **30**, 75.
19 M. Chen, Y. Lu, J. Fan, G.-C. Lv, Y. Zhao, Y. Zhang and W.-Y. Sun, *CrystEngComm*, 2012, **14**, 2015.
20 M. Chen, S.-S. Chen, T. Okamura, Z. Su, M.-S. Chen, Y. Zhao, W.-Y. Sun and N. Ueyama, *Cryst. Growth Des.*, 2011, **11**, 1901.
21 M. Zhu, S.-Q. Su, X.-Z. Song, Z.-M. Hao, S.-Y. Song and H.-J. Zhang, *Dalton Trans.*, 2012, **41**, 13267.
22 M. Chen, M.-S. Chen, T. Okamura, M.-F. Lv, W.-Y. Sun and N. Ueyama, *CrystEngComm*, 2011, **13**, 3801.
23 D. Lässig, J. Lincke and H. Krautscheid, *Tetrahedron Lett.*, 2010, **51**, 653.
24 A. Altomare, G. Cascarano, C. Giacovazzo, A. Guagliardi, M. C. Burla, G. Polidori and M. Camalli, *J. Appl. Crystallogr.*, 1994, **27**, 435.
25 P. T. Beurskens, G. Admiraal, G. Beurskens, W. P. Bosman, R. de Gelder, R. Israel and J. M. M. Smits, *The DIRDIF-99 program system, Technical Report of the Crystallography Laboratory*, University of Nijmegen, The Netherlands, 1999.
26 A. L. Spek, *J. Appl. Crystallogr.*, 2003, **36**, 7.
27 K. S. W. Sing, *Pure Appl. Chem.*, 1982, **54**, 2201.
28 S. Wang, Z.-W. Wei, J. Zhang, L. Jiang, D. Liu, J.-J. Jiang, R. Si and C.-Y. Su, *IUCrJ*, 2019, **6**, 85.

Received: 14th September 2020; Com. 20/6310